

Optimal seismic isolation characteristics for bridges in moderate and high seismicity areas

Xuan-Dai Nguyen^{1,2}, and Lotfi Guizani¹

¹*Department of Construction Engineering - Ecole de technologie supérieure, 1100 Notre-Dame St W, Montréal, Québec H3C 1K3, Canada*

²*Institute of Techniques for Special Engineering, Le Quy Don Technical University, Hanoi, Vietnam*

Corresponding Author: Lotfi Guizani

Department of Construction Engineering

Ecole de technologie supérieure, 1100 Notre-Dame St W, Montréal, Québec H3C 1K3, Canada

Abstract:

This paper aims to identify the optimal properties of Seismic Isolation Systems (SISs) for bridges in moderate seismicity areas (MSAs) and high seismicity areas (HSAs). Amplitude and spectral parameters of ground motions are proposed to identify these areas. A parametric study, with varying SIS properties, is carried out, and the seismic isolation performance is evaluated for several locations within MSAs and HSAs in North America and Europe. The optimal characteristic strength, Q_d , and post-elastic stiffness, K_d , of SISs are determined for each seismic area class to minimize seismic forces and displacement demands. Results indicate that ground motions for MSAs have a rich high frequency content, causing seismic spectra to vanish more rapidly with the elongation of the structure period. SISs with low-to-moderate energy dissipation capacities show the best performance for MSAs, while HSAs require SISs with higher damping capacities. Ranges for optimal Q_d and K_d of SISs for bridges in MSAs and HSAs are proposed.

Author keywords: Bridges, seismic isolation, ground motion characteristics, moderate seismic areas, optimal seismic isolation characteristics.

1. INTRODUCTION

During the last decades, the use of seismic protection devices, particularly seismic isolation systems (SISs), has grown in popularity for bridges in Canada, North America and worldwide (Guizani 2003; Morgan & Mahin 2011; Cheng & Shi 2018). These devices allow designing for a lower structural strength and externally provide a higher energy dissipation capacity that replaces the ductility required within the structure in the conventional capacity-based design seismic approach. In several seismic protection devices applications, the required ductility values ($R=20$ to 100) are much larger than the ductility capacities that traditional ductile structures can offer ($R=4, 5$) (Nicos Makris & Cameron J. Black 2004; CSA 2014). The basic principle of seismic base isolation consists in lowering the lateral stiffness of the bridge, thereby extending its fundamental period of vibration, which reduces the seismic forces transmitted to the structure. However, the period extension results in increased seismic displacement. To control the latter, SISs usually provide incorporated or external energy dissipation mechanisms, which increase the damping at the isolated period, typically by up to 30%.

Most current SISs can be classified as elastomer-based and friction-based, depending on their respective operating principles. Natural or high damping rubber bearings and lead-plug rubber bearings are the most popular elastomer-based SISs, whereas the friction pendulum is the most widely used friction-based SIS. (Dicleli & Buddaram 2006; Guizani & Chaallal 2011).

Two primary types of elastomer-based SISs (Lead-plug Rubber Bearing (LRB) and High Damping Rubber Bearing (HDRB) have traditionally been used over the decades, especially in North America. There is a third type, the Low Damping Rubber Bearing (LDRB), as well, but it is not commonly used as an SIS. However, over the last eighty years or so, it has largely been employed as a conventional bearing. Elastomer-based bearings provide a high vertical stiffness and bearing capacity, as well as a low horizontal and rotational stiffness, with a significant lateral restoring capacity. LRB provides the highest energy dissipation capacity, going up to 30%, based on the practically perfect elastoplastic behavior of lead in shear, with a low yield strength at ambient temperature (Buckle et al. 2006). The LRB system, however, suffers from shortcomings related to higher fabrication

costs and the presence of lead, which has negative environmental impacts. The HDRB system presents a non-linear behavior, with an interesting equivalent damping ratio varying between 10% and 15%, whereas the LDRB system exhibits a viscous linear behavior, with a low damping ratio of around 5% (Naeim & M. Kelly 1999). While the HDRB system would appear to provide a very good compromise in terms of damping, it nevertheless suffers from a higher sensitivity to cold and from the scragging phenomenon (Buckle et al. 2006). The LDRB system is simpler, less costly, and more reliable, but its damping capacity, while low, could be appropriate for MSAs.

The force-displacement behavior of a typical SIS is generally idealized by the bilinear model shown in Figure 1 (Naeim & M. Kelly 1999). The energy dissipation per cycle (EDC) is evaluated through the area under the hysteresis curve for a complete cycle at the design displacement, D_{\max} (Buckle et al. 2006).

Figure 1. Bilinear hysteresis model, typically used for seismic isolators

The bilinear model is a simplification of a wide variety of complex and coupled hysteresis behaviors associated with available seismic isolation systems. It shows deviations from more sophisticated models representing experimental results such as coupling of the horizontal direction, smoother and non-linear hysteresis behavior of elastomeric isolators (Constantinou et al. 1999; Fenz & Constantinou 2006; Becker & Mahin 2012), the impact of the vertical load, velocity and geometrical parameters on the hysteresis friction-based isolation systems. The equivalent bilinear model, therefore, can lead to slight differences in the seismic response of isolated structures (Eröz & DesRoches 2008; Eftychia Mavronicola & Komodromos 2014). However, these factors are considered an insignificant effect on determining the optimal range of general seismic isolation systems properties, especially when they are also affected by modification factors in practical designs. The equivalent bilinear model, therefore, is still considered a reliable model with reasonable accuracy and widely used for modeling isolated bridge structures. The main features of the bilinear behavior are the characteristic strength, Q_d , and the post-elastic stiffness, K_d , which govern the seismic response of base-isolated bridges (C. CSA 2014b). Other features, particularly K_u and F_y , are either related to the two or have little influence and/or vary within a limited range. Thus, the

performance of an SIS as evaluated by its efficiency in reducing the seismic demand in terms of force and displacement, F_{\max} and D_{\max} , is strongly dependent on its main features, Q_d , K_d , beyond the structure and earthquake characteristics. Generally, the post-elastic stiffness, K_d , plays a major role in controlling the lateral flexibility of the structure and the isolation period, while the characteristic strength, Q_d , is a key parameter related to energy dissipation and damping.

Earlier studies established that the seismic responses of base-isolated bridges are strongly affected by ground motion characteristics, especially the frequency content (Dicleli & Buddaram 2006; Zhang & Huo 2009; Huo & Alemdar 2010; Dicleli & Karalar 2011; Choun et al. 2014; Koval et al. 2016; Liu & Zhang 2016; Castaldo & Tubaldi 2018).

On the other hand, ground motion seismic characteristics vary considerably between Low Seismicity Areas (LSAs), Moderate Seismicity Areas (MSAs) and High Seismicity Areas (HSAs). We do not delve into LSAs in the present work since the seismic base isolation is typically not necessary. In MSAs, major earthquakes are relatively rare, but still pose a significant risk of devastating impacts on bridge structures. Therefore, in many countries, bridges in MSAs must be seismically designed even though this may be challenging (Nordenson & Bell 2000). While several studies have been carried out to evaluate the optimal characteristic properties of SISs, no systemic study has been performed to identify those of SISs for bridges, from an MSA and HSA classification perspective.

Mathematically, the frequency content of ground motion is highly correlated with the ratio of the peak ground acceleration (PGA) to the peak ground velocity (PGV). Dicleli and Buddaram (2006) demonstrated that the seismic force (F_{\max}), displacement demands (D_{\max}) and the energy dissipated by SIS hysteresis of base-isolated bridges are sensitive to variations of the PGA/PGV ratio. Increasing the PGA/PGV ratio results in a reduction of F_{\max} and D_{\max} . However, at very high PGA/PGV ratios, these reductions become negligible. Further, for ground motions with high PGA/PGV ratios, the effect of increasing Q_d is significant on F_{\max} , but marginal and non-salient on D_{\max} . For ground motions with low PGA/PGV ratios, the opposite picture is observed. The authors recommended using SISs with low

Q_d for seismic zones with high PGA/PGV ratios in order to minimize the force demand, while controlling the displacement demand.

Choun et al. (2014) investigated the effects of LRB properties on the seismic response of a base-isolated nuclear island excited by ground motions having different PGA/PGV ratios. In the study, the ground motions are classified into 3 groups: low ($PGA(g)/PGV(m/s) < 0.8$), moderate ($0.8 < PGA(g)/PGV(m/s) < 1.2$) and high ($PGA(g)/PGV(m/s) > 1.2$) PGA/PGV ratios. It was found that F_{max} and D_{max} decrease considerably as PGA/PGV increases. For ground motions with low PGA/PGV, F_{max} and D_{max} respectively reach up to 6 and 4 times equivalent demands for ground motion with moderate PGA/PGV ratios. For ground motions with high PGA/PGV ratios, F_{max} and D_{max} are practically unaffected by SIS property variations.

Park and Otsuka (1999) studied a simplified model of an isolated bridge under the El-Centro-1940 earthquake ground motion. The optimum Q_d , maximizing the energy absorbed by the SIS, was formulated in a linear relation of PGA.

Jangid (2007) optimized the elastic limit, F_y , of LRB for near-fault ground motions to minimize the superstructure acceleration and displacement. He proposed designing the LRB with F_y in the range of 0.15 to 0.2 times the superstructure weight, and with a value of K_d providing an isolation period in the 2.5-to-3.0 s range.

Zhang and Huo (2009) investigated optimal SIS parameters through a seismic fragility analysis. PGV was identified as the most appropriate ground motion intensity parameter affecting the seismic response, and consequently, fragility curves were proposed for damage levels as a function of PGV, instead of the usual PGA.

Dicleli and Karalar (2011) recommended higher Q_d values for ground motions with low PGA/PGV ratios, to minimize F_{max} and D_{max} , and an optimal value of K_d related to the value of Q_d .

RESEARCH OBJECTIVES AND METHODOLOGY

The main objective of this research is to identify the main SIS characteristics that are the most suited for MSAs and HSAs in general, and for eastern and western Canada, specifically. To this end, three specific end-goals are pursued:

- i. Find out common characteristics of earthquakes in MSAs and how they are distinct from those associated with HSAs.
- ii. Capture the effect of earthquake characteristics on SIS performance.
- iii. Identify the range of main SIS characteristics allowing near-optimal performances for locations in MSAs and HSAs, and more particularly, in North America and Canada.

To achieve the above objectives, seismic regions are grouped into 3 classes: low, moderate and high seismicity areas. Common features and differences in ground motions for each class are highlighted. Then, a parametric numerical study is carried out to evaluate the seismic responses of base-isolated bridges in MSAs and HSAs, while varying SIS characteristics. Optimal SIS characteristics, which minimize seismic demands, are then identified, for each seismic area class.

2. CLASSIFICATION AND GROUND MOTION CHARACTERISTICS OF EARTHQUAKE REGIONS

In this section, the classification of earthquake regions is generalized from earlier results of a global seismicity program based on the amplitude parameters of their ground motions. The ground motion characteristics, such as the frequency content and spectral parameters, are investigated to determine the common seismic base isolation-related features for each region.

Classification of earthquake regions

From 1992 to 1999, the United Nations conducted the Global Seismic Hazard Assessment Program (GSHAP) in a bid to mitigate seismic risk around the globe (Giardini 1999). The program allowed the development and implementation of a global seismic hazard map (GSHM), from which four hazard levels were proposed, varying from low to very high; they were then presented in regional maps with specific PGA values, for a probability of exceedance of 10% in 50 years, computed for reference rock conditions. The more recent Global Earthquake Model (GEM) (M. Paganì 2018) depicts the new geographic distribution of these PGA values, and extends and updates the scope of the work of the GSHAP to the risk domain. The seismic map resulting from the GEM was created by collating maps computed using national and regional probabilistic seismic hazard models.

Tarr et al. (2010) designed a scientific investigation map (SIM3064), which provided a comprehensive overview of Earth's seismicity from 1900 to 2007. The map also illustrated a global plate tectonics and the earth's physiography. It clearly identifies the location of large earthquakes and the rupture areas according to the 5.5-to-9.5 moment magnitude range, and provides a better understanding of the relative importance, the distribution, and the damaging potential of large earthquakes around the world.

According to these global maps, the Pacific Ring of Fire and Alpine-Himalayan Belt are known as two world's regions of high seismicity. In the present paper, we classify these regions as HSAs. They include West North America and Southeast Europe, where PGAs, with a probability of exceedance of 10% in 50 years, are typically greater than 0.2 g. Meanwhile, other seismic regions, such as East North America and Northwest Europe, have a relatively lower rate of earthquake activity. Most of the locations in these regions have PGAs, with a probability of exceedance of 10% in 50 years, from 0.08 g to 0.2 g; these are classified as MSAs. LSAs are areas where PGAs, for the same probability of exceedance, are less than 0.08 g. LSAs in which the seismic base isolation is considered unnecessary, as well as some other earthquake regions, such as Japan and New Zealand, are not examined in this study.

Ground motion characteristics in HSAs and MSAs

While the classification and the maps presented in the last section provide a critical zonation for macro planning and engineering, other important properties of earthquakes, such as frequency content and spectral parameters, which are of prime importance for seismic design, have not been considered.

In this section, the main characteristics of ground motions affecting the seismic response of base-isolated bridges are identified, based on a literature review, and examined for each zone. Several earthquake regions with different levels of seismic activity are considered, notably North America and Europe. The amplitude and spectral parameters for these regions are derived on the basis of their design standards, in particular: Eurocode8 (ECS 2005a), the Canadian Highway Bridge design code, CSA-S6 (CSA 2014), the National Building Code of Canada 2015,

NBCC-2015 (NRCC 2015), the American Society of Civil Engineers (ASCE-7 2016), and the AASHTO - LRDF Bridge Design Specifications (AASHTO 2017).

As pointed out by earlier studies, the PGA/PGV is a very good parameter used to characterize the frequency content of a given earthquake signal (Kramer 1996; Dicleli & Buddaram 2006), while the energy content can be represented by the ratio of spectrum values for short periods to long periods (C. CSA 2014b). These parameters, extracted from the applicable standards for each region, are used in this study to investigate the frequency content and the energy content.

Eurocode8 (EC8) (ECS 2005a), largely used in Europe, Asia and Africa, distinguishes between two types of spectral shapes based on the characteristics of the most significant earthquakes contributing to local hazards, namely, Type 1, used for HSAs, such as Southeast Europe (south Italy, Turkey, Greece, etc.), and far-field earthquakes, which carry more energy in the long periods range, and Type 2, recommended for LSAs and MSAs, such as Northwest Europe (France, Belgium, Germany, Switzerland, etc.) and near-field earthquakes having less energy in the long periods range and larger amplitudes at shorter periods (Solomos et al. 2008; Trifunac & Todorovska 2012; Elghazouli 2016).

The frequency content of the two seismicity areas covered by EC8 spectra types are investigated through the PGA/PGV ratio, with the PGA calculated by:

$$PGA = a_g S \quad (1)$$

where a_g is the peak ground acceleration on rock with a probability of exceedance of 10% in 50 years and S is the site amplification factor. The PGV is a function of the elastic acceleration spectrum ordinates at periods 0.2 s ($S_{0.2}$) and 1.0 s ($S_{1.0}$) (Paolucci & Smerzini 2018).

$$PGV = 0.75 \left(\frac{S_{0.2}}{g} \frac{S_{1.0}}{g} \right)^{0.55} \quad (m/s) \quad (2)$$

Based on the SHARE project databases (Giardini et al. 2014), some locations in Northwest Europe and Southeast Europe are selected to examine earthquake characteristics for European MSAs and HSAs.

In North America, two distinct earthquake regions are identified. The West Coast, a part of the Pacific Ring of Fire, known as the most earthquake-prone area of

North America, is classified as an HSA. The East Coast, located on a stable continental region, has a lower rate of earthquake activity, and is classified as an MSA. Earlier studies found considerable differences in the ground motion characteristics of West North America and East North America, with more energy concentrated at higher frequencies in East North America and affecting shorter period structures more significantly, as compared to West North America (Anderson et al. 2008; Atkinson 2009; CSA 2014).

The PGA and PGV values for locations in Canada are determined by Natural Resources Canada (NRC 10 June 2019) while those for the United States (US) are determined by the US Geological Survey (USGS 9 June 2019). PGV values for the US are estimated by (Anderson et al. 2008):

$$PGV = 55F_v S_1 \quad (in/s) \quad (3)$$

where F_v is the site amplification factor and S_1 is the spectral acceleration in units of g, at 1.0 s.

Based on the above, the PGA/PGV ratios are evaluated for a 10% probability of exceedance in 50 years, for many locations in Europe and North America and presented in Table 1.

As shown in Table 1, the PGA/PGV ratios for MSA locations are about 1.5 to 2 times higher than for HSAs because of the richer content in high frequencies of the former.

Some sub-regions within MSAs, such as the Charlevoix region in Quebec (East North America), which is normally considered an HSA according to the USGS classification, by the PGA (USGS 9 June 2019), may present a high seismic activity. Nevertheless, the earthquake characteristics of this sub-region, such as the frequency content, are similar to those obtained for other East North America locations, classified as MSAs. Consequently, findings obtained for MSAs should apply to such sub-regions, with due consideration to the intensity of the earthquakes.

On the other hand, the spectrum shape also represents differences in earthquake energy concentration in the frequency domain. The design spectrum for specific locations in North America and Europe, according the current applicable code, is

investigated below, with a 10% exceedance probability in 50 years. Figure 2.a) shows the EC8 spectra for Turin and Napoli, Italy, located in an MSA and HSA, respectively, for a type B soil. The figure illustrates large differences in spectral values in the long periods range, not only because of the seismic intensity, but also because of the spectra shapes. This is evident when comparing the Turin and Napoli spectra scaled for the same PGA.

Similarly, the spectral parameters are investigated for North America. In Canada, the CSA-S6-14 introduced major changes in the design spectra over the preceding edition (S6-06), reflecting the recognized differences in earthquake ground motion characteristics between eastern and western seismic areas (C. CSA 2014b; Koval et al. 2016).

Figure 2.b) illustrates the spectral accelerations calculated by S6-14 and S6-06 for Montreal (East North America) and Vancouver (West North America), Canada. While S6-06 adopts the same spectrum for both cities, S6-14 specifies quite different spectra, with very distinct shapes for the two locations. This change, especially at long periods, is very meaningful for the design of isolated bridges. For example, at the Montreal location, the spectral acceleration at 2.0s decreased considerably, going from 0.126 g in S6-06 to 0.024 g in S6-14. Meanwhile, at the Vancouver location, this spectral value changed only slightly, to 0.117 g in S6-14. In the United States, the spectra shapes calculated by AASHTO (2017) present clear differences between the West and East Coast regions. Figure 2.c) shows the acceleration spectra for different eastern and western locations.

The earthquake regions in Mexico are clearly distinguished in terms of seismic intensity (PGA); the east coast is classified as an MSA, while the west coast, a region within the Pacific Ring, corresponds to an HSA (MDOC 2015). Figure 2.d) shows the design spectra for Mexico City (HAS) and Monterrey (MSA). However, a close examination of the design spectra for both regions indicates that the same spectrum shape applies for locations within both regions. The design spectra for Mexico have a distinctive shape, with a plateau extending up to 1.4 s, and a very small acceleration reduction between short periods and periods around 2.0 s. This is probably explained by the fact that the Mexican code was extended from the code developed for Mexico City, the highest seismic zone according to a

traditionally defined seismic hazard (Ordaz & Meli 2004; Alcocer & Castaño 2008). Hence, MSAs in Mexico could very well differ from those of East North America, and consequently, the general conclusions drawn for East North America and MSAs may not strictly apply to the east of Mexico. Further, because of the particular spectrum shape for Mexico, the seismic base isolation in Mexico would seem to be inappropriate for isolation periods around 2.0 s, as there is no force reduction between short periods and 2.0 s. The seismic base isolation in Mexico requires special consideration, and is not further addressed in the present paper. Figure 2. Design spectra with a probability of exceedance of 10% in 50 years: a) Italy (ECS 2005a); b) Canada (CSA 2014); c) United States (AASHTO 2017); and d) Mexico (MDOC 2015)

The spectral acceleration and displacement ratios at 0.2 s and 2.0 s [$R_a = S_a(0.2)/S_a(2.0)$] and [$R_d = S_d(2.0)/S_d(0.2)$] are used to represent the spectrum shape. These spectral ratios are also pertinent to force reduction and displacement increase due to period extension by seismic isolation. Table 2 shows the computed values of these ratios for many locations in Europe and North America, within MSAs and HSAs.

As observed, R_a ratios in the MSAs are much larger (about twice or more) than in the HSAs for all the locations considered in Europe and North America. In other words, the elongation of the vibration period from 0.2 s to 2.0 s by the seismic base isolation causes a much larger force reduction (about twice or more) in MSAs than in HSAs. Conversely, R_d ratios in MSAs are much smaller than in HSAs (about half and less), indicating that the relative increase in seismic displacement due to period elongation by the seismic base isolation, is considerably less significant for locations in MSAs. Figure 3 illustrates a histogram chart of the ground motion characteristics discussed above in the locations considered on the background map of GEM's GSHM. Similar trends for the two seismic classes (MSA and HSA) in Europe and North America are obvious: compared to HSAs, earthquakes in MSAs are characterized by a richer high frequency content (represented by a higher PGA/PGV), a larger seismic force reduction due to the period elongation (associated with a higher R_a) and a much lower displacement increase due to period elongation (lower R_d).

Figure 3. Ground motion characteristics in North America and in Europe, background map from GEM (M. Pagni 2018)

3. PARAMETRIC STUDY

A parametric study is carried out in order to investigate the effect of earthquake ground motion characteristics on the seismic force and displacement demands as a function of SIS characteristics. MSA and HSA locations, subject to three earthquake design standards AASHTO (AASHTO 2017), EC8 (ECS 2005a), and S6-14 (CSA 2014) are considered. SIS performances are measured through the maximum values of lateral force (F_{max}), displacement (D_{max}) and the residual displacement, D_r , when available.

Studied parameters

Two types of parameters are considered, namely, SIS characteristics and earthquake ground motion characteristics. The characteristic strength, Q_d , and the post-elastic stiffness, K_d , are the principal SIS characteristic parameters considered. The values of Q_d and K_d , obtained through the Q_d/W and K_d/W ratios, are varied to cover the practical range parameters of SIS designs conforming to the current available commercial SIS types (Naeim & M. Kelly 1999; Dicleli & Buddaram 2006) and in the applicable codes. The initial stiffness, K_u , which is not considered as a main parameter, is varied within a limited number of possibilities. Table 3 presents the range of the studied SIS parameter values.

The earthquake characteristics are considered in this parametric study through the use of the design spectra for different MSA and HSA locations. These are broken down as follows: West North America, East North America, Southeast Europe and Northwest Europe. Boston (MA, US), Turin (Italy, EC8-type 2), and Montreal (QC, Canada) are locations selected to represent MSAs, whereas HSAs are represented by Portland (OR, US), Napoli (Italy, EC8-type 1) and Vancouver (BC, Canada).

Modelling of base-isolated bridges

Typically, seismic isolation is used on bridges with relatively stiff substructures. In such cases, the effects of the bridge substructure stiffness may be ignored or included in the initial SIS stiffness, K_u . Further, the bridge superstructure is considered as a horizontal rigid diaphragm so that, considering only the

longitudinal direction, all the isolation units experience the same displacement, and their properties can therefore be lumped into a single equivalent isolation unit representing the SIS. The bridge can therefore be modeled as a single-degree-of-freedom system (SDOF), as illustrated in Figure 4. The substructure mass can be reasonably ignored or taken into account by adjusting the superstructure mass (Leroux et al. 2017). The vertical ground motion component has not been taken into account as it does not affect significantly the horizontal response of the bridge, which is of prime importance (Button et al. 2002; Tubaldi et al. 2018).

Figure 4. Typical seismic-isolated bridge and SDOF model

The hysteretic behavior of most available seismic isolators can be idealized by a bilinear force-displacement relationship (Buckle et al. 2006; Dicleli & Buddaram 2006; C. CSA 2014b). Typically (Figure 1), the elastic stiffness, K_u , is so high that the yield displacement D_y is nearly equal to 0, and therefore, it has no practical noticeable effects on the response of isolated bridges (Nicos Makris & Cameron J Black 2004; Dicleli & Buddaram 2006).

Seismic analysis methods

Two analysis methods are used on the SDOF bridge models: 1) spectral analysis through an iterative procedure, on the equivalent visco-elastic SDOF model, herein referred to as single mode spectral analysis (SMSA), and 2) nonlinear time history analysis (NLTHA), on the SDOF, using the bilinear hysteretic behavior presented in Figure 1. In some specifications, NLTHA is also referred as “nonlinear response history analysis - NLRHA” (ASCE-7 2016; ATC-58 2018), “nonlinear dynamic analysis - NDA” (NRCC 2015) or “nonlinear dynamic procedure - NDP” (ASCE/SEI-41-13 2014).

a. Single Mode Spectral Analysis: SMSA

The SMSA method is mainly used in a parametric study to estimate the optimal characteristics of SISs, as well as to predict the seismic response of isolated bridges in the different seismic areas (MSA, HSA). This method uses an equivalent linear SDOF system with viscous damping calculated at the design displacement, D_{max} , of the nonlinear system. As illustrated in Figure 1, the substructure and the isolation system stiffness are represented by the effective stiffness, K_{eff} , and the energy dissipated by the hysteresis loop is represented by

an equivalent viscous damper with a damping ratio, β_{eff} (Chopra 2017). The seismic displacement, which must match the design spectrum and the bilinear behavior, is unknown, and an iterative procedure is used to establish it (Buckle et al. 2006; Guizani 2007; Jara et al. 2012; Koval et al. 2016). Figure 5 shows the scheme used for a given bridge weight (W), and SIS properties, Q_d , K_u and K_d .

Figure 5. SMSA scheme for base-isolated bridges with stiff substructures
In total, 1053 base-isolated bridges (SISs) were analyzed for each of the six locations (6318 analyses).

b. Non-Linear Time History Analysis: NLTHA

To prevent significant errors, which could lead to unsafe designs, the codes limit the application of SMSA to a range conforming to certain conditions, notably relating to the equivalent damping, the effective period and the restoring capacity (ECS 2005a; CSA 2014; AASHTO 2017). Outside the SMSA validity range, NLTHAs are required for computing the seismic demand on base-isolated bridges. NLTHAs, which are more demanding, are used here in a limited fashion to complement and validate the results of the SMSA. They allow extending the parametric study beyond the range of validity of the SMSA and obtaining additional results, such as the residual displacement.

The Canadian cities of Montreal and Vancouver, representing the two highest seismic risk areas in Canada (Adams & Halchuk 2004), are chosen to represent the two seismic area classes, MSA and HSA, respectively. For each location, a suite of 48 scaled orthogonal artificial ground motions and 6 historical orthogonal ground motions were used. The six historical orthogonal ground motions correspond to three pairs of recorded ground motions which have readably transformed into two horizontal orthogonal axes (Penzien & Watabe 1974) and then scaled to the design spectra (CSA 2014; Tremblay et al. 2015) for a probability of exceedance of 2% in 50 years, type C soil and 5% damping, with the SeismoMatch software (SeismoSoft 2016).

Historical ground motions, presented in Table 5, are obtained from Natural Resources Canada (NRC 10 June 2019), and scaled by one scenario in the 0.2s to 6.0s period range. Artificial ground motions are selected from the Atkinson Database (Atkinson 2009) according to two scenarios, and scaled within the

specific scenario range shown in Table 4. Wide scaling period ranges are used, covering the contribution of the elastic (initial) and inelastic response phases of SISs on the studied base-isolated bridges. It should be noted that the scaling range (0.1 to 6.0s) covers the entire range of the effective periods of all the studied bridges. Further, the scaled spectra for all ground motion records used do not drop below 10% of the design spectra. Based on these observations, the global average values of the maximum seismic demands are used, as expected demands.

As shown in Figure 6.a) and b), an excellent match is obtained between the mean spectra of the selected and scaled ground motions and the design spectra for both locations.

Figure 6. Mean spectra of scaled historical ground motions and design spectra:

a) Vancouver, b) Montreal

The NLTHA of the SDOF nonlinear model, shown in Figure 4, with a wider range of Q_d/W (from 0.01 to 0.2) and K_d/W (from 0.025 m^{-1} to 5 m^{-1} , accordingly, $\mu=0.001$ to 0.2) were conducted to cover all possible SIS types within and outside the specified limits by the design codes for SMSA. An overall total of 38200 SISs were each generated and analyzed under 54 ground motions for each of the two locations, resulting in more than 4×10^6 NLTHA.

Effects of SIS characteristics on the seismic response

Figure 7.a) and b) shows the variation of F_{\max} and D_{\max} , obtained by SMSAs, as a function of Q_d/W for isolated bridges with a constant, K_d ($K_d/W=2.5 \text{ m}^{-1}$), at the six considered locations. As shown in Figure 7.a), the seismic force demands, for the two seismic areas (HSA and MSA), follow opposite tendencies with increasing Q_d/W . While for HSA sites, F_{\max}/W decreases with increasing Q_d/W , for MSA sites, this tendency is valid only for low values of Q_d/W , and is inverted beyond a certain threshold in the 0.02 to 0.04 range, where F_{\max}/W increases at an almost constant rate with increasing Q_d/W .

Figure 7.b) shows that D_{\max} follows the similar general tendency for both seismic areas: D_{\max} decreases with increasing Q_d/W . However, the magnitude of D_{\max} and the rate of its decrease are much lower for MSAs. In fact, for MSAs, beyond a

Q_d/W threshold of about 0.03 to 0.04, the seismic displacement demand for MSA remains practically constant with increasing Q_d/W .

Combining the results of Figure 7.a) and b) suggests that moderate and relatively small values of Q_d/W , in the 0.02 to 0.04 range, are more efficient for isolated bridges in MSAs as they lead to a minimum F_{max} and maintain D_{max} near a minimum. In contrast, higher values of Q_d/W are recommended for bridge SISs in HSAs, specifically to decrease D_{max} below tight limits.

Similarly, the effects of the post-elastic stiffness, K_d , on the seismic demand in terms of F_{max} and D_{max} are presented in Figure 7.c) and d). The results of both earthquake regions present a similar tendency: increasing K_d/W results in an increase of F_{max} and a decrease of D_{max} . However, the effects of K_d variation on F_{max} and D_{max} are much less significant for MSAs than for HSAs. For MSAs, with increasing K_d , only a slight increase in force demand is observed, while the displacement demand is practically constant. Furthermore, we clearly observe that force demands, and particularly displacement demands, for MSAs are significantly lower than for HSAs for all values of K_d .

Figure 7. Effect of various isolator parameters on F_{max} and D_{max} : a) Q_d/W on F_{max} with $K_d/W=2.5 \text{ m}^{-1}$; b) Q_d/W on D_{max} with $K_d/W=2.5 \text{ m}^{-1}$; c) K_d/W on F_{max} with $Q_d/W=0.05$; and d) K_d/W on D_{max} with $Q_d/W=0.05$

Based on the above, we can note that for MSA locations, the effect of K_d on seismic demand is very minor, and therefore, it is generally preferable to choose a small value of K_d .

For HSA locations, the effect of K_d is significant, and trends in opposite directions for F_{max} and D_{max} . No optimal range is identified, and K_d is chosen on a case-by-case basis, depending on specific case constraints, in order to ensure the best tradeoff between displacement and force optimization. To minimize F_{max} , using high values of Q_d and low values of K_d is more appropriate, while to minimize D_{max} , using high values of Q_d with relatively high values of K_d is recommended.

Nevertheless, for both locations, the choice of K_d has to take into account the residual displacement. Too small values of K_d may cause large displacements and may cause inadequacy of the SMSA results, as discussed later. However, the SMSA method is applied only with its established domain of validity which is

defined by certain conditions on the effective period, damping ratio, restoring capability, etc. (CSA 2014). Furthermore, inside of the limitation, the SMSA often provides a conservative (overestimated) prediction of the seismic demand for design purposes (E Mavronicola & Komodromos 2011; Koval et al. 2016). Therefore, the NLRHA shall be performed to validate these findings.

Validation and extension of SMSA results by NLTHA

Figure 8 presents seismic force demands and displacement demands, obtained by NTLHAs, as functions of Q_d/W , for different discrete values of K_d/W , for the Vancouver and Montreal sites. Similar trends as those obtained with SMSA (Figure 7) are observed. Results confirm that the seismic force demand, F_{max}/W , reaches a minimum value for a Q_d/W ratio in the range of 0.02 to 0.04 for isolated bridges in Montreal (MSA) and 0.08 to 0.12 in Vancouver (HSA).

Figure 8. Effect of Q_d/W with different K_d/W on F_{max} and D_{max} for isolated bridge:

a), c) Vancouver; b), d) Montreal, (K_d/W in m^{-1})

Regarding the seismic displacement demands, D_{max} (Figure 8.c) and d)), similar trends as those observed from SMSA results are also obtained, with D_{max} generally decreasing as Q_d/W increases. However, the reduction rates of D_{max} with increasing Q_d/W are much lower for Montreal than for Vancouver.

It is also observed from Figure 8.d) that for isolated bridges in Montreal, when $Q_d/W > 0.06$, D_{max} is nearly constant, and is not affected by either K_d/W or Q_d/W . Hence, the selection of a high value of Q_d/W is not only less effective in reducing D_{max} , but also significantly increases F_{max} , as shown in Figure 8.b), and should be discouraged for this location.

As shown in Figure 8.c), for bridges in Vancouver, small values of Q_d/W ($Q_d/W \leq 0.04$) seem to be inappropriate as they lead to large seismic force and displacement demands. On the other hand, for Q_d/W higher than 0.12 ($Q_d/W > 0.12$), F_{max} increases with a Q_d/W increase (Figure 8.a)), while D_{max} remains almost constant (Figure 8.c)). It follows that values of Q_d/W in the range of 0.08 to 0.12 ($0.08 \leq Q_d/W \leq 0.12$) are the most appropriate for the Vancouver site. Similarly, the effects of K_d/W on F_{max} and D_{max} are investigated through the results presented in Figure 9 for the studied locations.

Figure 9. Effect of K_d/W with different Q_d/W on F_{max} and D_{max} for isolated bridges: a), c) Vancouver; b), d) Montreal

The general trends and results obtained are very similar to those obtained with SMSA. Generally, F_{max} increases and D_{max} decreases with increasing K_d/W . However, as observed with SMSA results, seismic demands in Vancouver are much more affected by the K_d/W ratio than in Montreal. High values of K_d/W ($K_d/W > 4 \text{ m}^{-1}$) are not favorable as they result in an increase of F_{max} , with D_{max} being nearly constant. On the other hand, too small values of K_d/W lead to large displacements, especially with small Q_d/W .

To allow a direct comparison with NLTHA, results obtained with SMSA, for an average specific value of $K_d/W = 2.5 \text{ m}^{-1}$, are included in Figure 8 and Figure 9. It is observed that despite the similar trends in the results, SMSA predicts higher and conservative seismic force and displacement demands.

The residual displacement (D_r), a permanent shift (offset) of the superstructure and meaningful about functionality and repair costs (reentering the bridge), is investigated in Figure 10.

Figure 10. Effect of K_d/W with different Q_d/W on D_r for isolated bridge: a) in Vancouver; b) in Montreal

For both locations, the residual displacement, D_r , decreases significantly as K_d/W increases. SISs with small values of K_d/W lead to very high values of D_r , especially for isolated bridges in Vancouver. The residual displacement increases slightly with increasing Q_d/W . The authors propose a lower value of $K_d/W = 0.5 \text{ m}^{-1}$, to limit the residual displacement to 6 mm for Montreal and 15 mm for Vancouver.

4. OPTIMAL SIS CHARACTERISTICS FOR MAIN CANADIAN EARTHQUAKE ZONES

Optimization of Q_d and K_d based on minimizing F_{max}

Based on the NLTHA results for the Vancouver and Montreal sites, for any value of K_d , the associated optimal value of Q_d minimizing F_{max} is determined. Then, a statistical distribution of the optimal Q_d/W is constructed, covering the studied range of K_d/W . To generalize the results to include relatively stiff substructures without neglecting their flexibility, the results are presented in terms of the elastic period of the structure which is calculated with the elastic stiffness, K_e . The latter

is obtained by combining the substructure stiffness, K_{sub} , in series with the initial stiffness of the isolation system, K_u , and is given by:

$$K_e = \frac{K_u K_{sub}}{K_u + K_{sub}} \quad (4)$$

To ensure that a larger range is covered, additional values of K_e are considered so that the elastic periods, T_e , are [0.20s; 0.25s; 0.30s; 0.34s; 0.40s; 0.45s]. Then, a parametric study is conducted, where the values of K_d , Q_d and K_e are varied as indicated in Table 6. For each combination of these parameters, a NLTHA, as described above, is carried out, for both the Montreal and Vancouver locations. In total, just over 9.9×10^6 NLTHAs on the bilinear SDOF shown in Figure 4 are undertaken for each location.

Figure 11.a) and b) shows the statistical distributions of optimal values of Q_d/W for Vancouver and Montreal, respectively. The histograms in grey represent all the values of K_d/W while the highlighted ones represent the values of K_d within the range of practical interest: $0.5 \text{ m}^{-1} \leq K_d/W \leq 4.0 \text{ m}^{-1}$. Values outside this latter range are either too small, and cause large residual displacements, or too high, and not of practical interest as the isolation period should be lower than 1.0 s.

Figure 11. Statistical distribution of Q_d/W minimizing F_{max} for isolated bridges: a) in Vancouver (HSA), b) in Montreal (MSA)

As shown in Figure 11.a), for isolated bridges in Vancouver with a practical range, K_d/W , all the minimum values of F_{max} are obtained for Q_d/W ranging from 0.06 to 0.14, with a concentration in the 0.08 to 0.12 range. Similarly, for isolated bridges in Montreal (Figure 11.b), Q_d/W varies from 0.01 to 0.05, and concentrates primarily in the 0.015 to 0.045 range. These findings are consistent with earlier conclusions.

The graphs of optimal values of Q_d/W for different elastic periods, T_e , are shown in Figure 12 a) and b).

Figure 12. Optimal Q_d/W , minimizing F_{max} , as a function of K_d/W

These results show a strong correlation between the optimal values of Q_d/W and K_d/W ratios. Optimal values of Q_d/W increase practically in a linear manner with k_d/W . Linear regressions, with very high coefficients of determination (R^2) are fitted

to express the optimum Q_d/W as a function K_d/W , for different elastic periods, T_e , for both the Montreal and Vancouver locations (see Figure 12).

The overall linear relations for the optimum Q_d/W , minimizing F_{\max} as a function of K_d/W for Vancouver and Montreal are given by Eq.(5) and Eq.(6), respectively:

$$Q_d/W = 0.0141 K_d/W + 0.0675, R^2 = 0.7514 \quad (5)$$

$$Q_d/W = 0.0077 K_d/W + 0.0136, R^2 = 0.9318 \quad (6)$$

It is interesting to note that for Montreal, Eq.(6) above has a very high R^2 as the results of Figure 12.b) show low scatter of the optimal value of Q_d/W when K_d/W varies. This is explained by the fact that the optimum Q_d/W is barely affected by the elastic period. Therefore, it is believed that a single regression equation is very adequate for all values of T_e within the studied range. Conversely, for Vancouver, a lower R^2 is obtained for the overall Eq.(5), because the effect of the elastic stiffness, K_e , on the optimal Q_d/W is more significant. Consequently, using the regressions of Figure 12.a) for specific elastic periods, T_e , is considered more appropriate ($R^2 \geq 0.91$).

Optimal equivalent viscous damping ratios

In this section, the optimal values of Q_d/W are expressed in terms of equivalent linear viscous damping ratio, β_{eff} :

$$\beta_{\text{eff}} = \frac{EDC}{2\pi K_{\text{eff}} D_{\text{max}}^2} = \frac{4Q_d (D_{\text{max}} - D_y)}{2\pi (Q_d + K_d D_{\text{max}}) D_{\text{max}}} \quad (7)$$

Neglecting the displacement at yield, D_y (K_e infinite), the following relation is obtained:

$$\beta_{\text{eff}} \approx \frac{4Q_d}{2\pi (Q_d + K_d D_{\text{max}})} \quad (8)$$

Figure 13.a) shows a few relations obtained for both locations.

Figure 13. Equivalent viscous damping ratios for Vancouver and Montreal: a) optimal ratios calculated at associated design displacement; b) damping ratios for optimal solutions variation with locality

From Figure 13.a), the optimal damping ratios for Vancouver are typically in the 25% to 35% range, and depend on K_d and T_e . For Montreal, the optimal viscous

damping ratios are lower, and range generally from 20% to 25%, with a lower dependency on K_d and T_e .

Nevertheless, notwithstanding the fact that optimal damping ratios for Montreal are lower than those for Vancouver, the results of Figure 13.a) are not very indicative of the real damping capacities of optimal SISs for both locations. This is because the damping ratios presented are not calculated for the same maximum seismic displacement, D_{max} . As indicated by Eq.(8), for the same SIS (Q_d and K_d), when D_{max} decreases, the equivalent damping ratio increases. Consequently, because the D_{max} values are much lower for Montreal than for Vancouver, optimal damping ratios obtained for both locations are relatively close. However, in reality, optimal SISs associated with Vancouver have much greater damping capacities than those associated with Montreal. To illustrate this difference, the damping ratios with the midrange optimal values of Q_d/W for both locations are calculated and compared at the same location, as shown in Figure 13.b).

Results clearly indicate that typical optimal SIS calculated for the same location show much lower damping ratios for Montreal than for Vancouver, and vice-versa. For example, an SIS with $Q_d/W=0.03$, optimal for Montreal, shows a very low damping ratio ranging from 5% to 12% when used in Vancouver, despite its calculated damping ratio ranging from 17% to 40% when used in Montreal. Comparatively, an SIS with $Q_d/W=0.1$, which is typically optimal for Vancouver, shows a damping ratio ranging from 20% to 45%. Calculated for the same displacement, optimal SISs for Montreal dissipate about 3 times less energy than those for Vancouver.

5. CONCLUSIONS AND RECOMMENDATIONS.

In this research, the common earthquake characteristics of MSAs and HSAs are studied through amplitude and spectral parameters. Classifications of earthquake regions for North America and Europe are conducted based on the background map from GEM (M. Paganì 2018). The effects of earthquake characteristics on SIS performances are investigated through SMSAs and validated through NLTHAs. Additionally, the optimum characteristic strength, Q_d , and post-elastic stiffness, K_d , are evaluated for isolated bridges in MSA and HSA in general, and

Montreal and Vancouver, Canada, more specifically. The following conclusions are drawn:

1. PGA/PGV ratios for locations in MSAs are approximately twice as large as those in HSAs.
2. The design spectra shapes for MSAs vanish more rapidly with period elongation, making the seismic base isolation more effective in MSAs than in HSAs.
3. For isolated bridges in MSAs, increasing the characteristic strength, Q_d , beyond a certain threshold results in an increase of the seismic force demand, F_{max} . Consequently, small to moderate values (0.02 to 0.04) of Q_d/W are the most appropriate.
4. For isolated bridges in HSAs, F_{max} decreases with increasing Q_d , up to an upper limit of about 0.12W to 0.14W, beyond which the seismic force increases with increasing Q_d . With respect to seismic force demand, the optimum values of Q_d range from 0.08 to 0.12 W.
5. The post-elastic stiffness, K_d , influences D_{max} and F_{max} in opposite ways. Generally, F_{max} increases and D_{max} decreases with increasing K_d . However, these effects are more accentuated for isolated bridges in HSAs, while they are practically negligible for bridges in MSAs. Nevertheless, too small values of K_d lead to large values of D_{max} and D_r , while too high values of K_d result in less effective SISs as the F_{max} increases, with only a negligible reduction in D_{max} .
6. Based on extensive NLTHA results, the optimal characteristics of SISs for Montreal and Vancouver are identified: Q_d/W in the range of 0.015 to 0.045 for Montreal and 0.08 to 0.12 for Vancouver. Regression expressions are proposed for a more accurate estimate of optimal Q_d/W as a function of K_d/W .
7. Optimal values of K_d/W in the range of 0.5 m^{-1} to 4 m^{-1} for both locations are recommended. Values at the lower limit are preferred, especially for Vancouver, in order to restrain the seismic force demand, F_{max} .
8. Values of K_d/W higher than 0.5 ensure controlling the residual displacement under 6 mm for Montreal and 15 mm for Vancouver.
9. Optimal viscous damping ratios for both locations range typically from 20% to 25% in Montreal and 25% to 30% in Vancouver. However, because these ratios

depend on the design displacement, D_{\max} , which is much higher for Vancouver (twice or more), they are not very representative of the real energy dissipation capacities of optimal systems in both regions. Values of Q_d/W are more indicative in this regard. Typical optimal SISs for Montreal, with Q_d/W around 0.03, have only 5% to 12% damping ratios when calculated for Vancouver.

References

- AASHTO. 2017. AASHTO LRFD Bridge Design Specifications 8th Edition. *American Association of State Highway and Transportation Officials, Washington, DC.*
- Adams, J., & Halchuk, S. 2004. *Fourth-generation seismic hazard maps for the 2005 national building code of Canada.* Paper presented at the Proceedings of the 13th World Conference on Earthquake Engineering, Vancouver, Canada. Paper.
- Alcocer, S. M., & Castaño, V. M. 2008. Evolution of codes for structural design in Mexico. *Structural Survey*, 26(1), 17-28.
- Anderson, D., Martin, G., Lam, I., & Wang, J. 2008. NCHRP Report: 611: Seismic Analysis and Design of Retaining Walls, Buried Structures, Slopes, and Embankments. *Transportation Research Board Project*, 12-70.
- ASCE-7. 2016. ASCE Minimum Design Loads and Associated Criteria for Buildings and Other Structures. In: American Society of Civil Engineers.
- ASCE/SEI-41-13. 2014. *Seismic evaluation and retrofit of existing buildings.*
- ATC-58. 2018. Seismic Performance Assessment of Buildings, Applied Technology Council. In.
- Atkinson, G. M. 2009. Earthquake time histories compatible with the 2005 National building code of Canada uniform hazard spectrum. *Canadian Journal of Civil Engineering*, 36(6), 991-1000.
- Becker, T. C., & Mahin, S. A. 2012. Experimental and analytical study of the bi-directional behavior of the triple friction pendulum isolator. *Earthquake Engineering & Structural Dynamics*, 41(3), 355-373.
- Buckle, I., Constantiou, M., Dicleli, M., & Ghasemi, H. 2006. *Seismic isolation of highway bridges*: MCEER, University at Buffalo, the State University of New York.
- Button, M. R., Cronin, C. J., & Mayes, R. L. 2002. Effect of vertical motions on seismic response of highway bridges. *Journal of Structural Engineering*, 128(12), 1551-1564.
- Castaldo, P., & Tubaldi, E. 2018. Influence of ground motion characteristics on the optimal single concave sliding bearing properties for base-isolated structures. *Soil Dynamics and Earthquake Engineering*, 104, 346-364.
- Cheng, Z., & Shi, Z. 2018. Composite periodic foundation and its application for seismic isolation. *Earthquake Engineering & Structural Dynamics*, 47(4), 925-944.
- Chopra, A. K. 2017. Dynamics of structures. theory and applications to earthquake engineering.
- Choun, Y.-S., Park, J., & Choi, I.-K. 2014. Effects of mechanical property variability in lead rubber bearings on the response of seismic isolation system for different ground motions. *Nuclear Engineering and Technology*, 46(5), 605-618.
- Constantinou, M. C., Tsopelas, P., Kasalanati, A., & Wolff, E. D. 1999. Property modification factors for seismic isolation bearings.

- CSA. 2014. Code canadien sur le calcul des ponts routiers. In (pp. lv, 885). [11e éd.]. -- Mississauga, Ont.: Groupe CSA.
- CSA, C. 2014b. Standard S6-14. *Commentary on CSA S6-14, Canadian Highway Bridge Design Code, Canadian Standards Association, Mississauga, ON.*
- Dicleli, M., & Buddaram, S. 2006. Effect of isolator and ground motion characteristics on the performance of seismic-isolated bridges. *Earthquake Engineering & Structural Dynamics*, 35(2), 233-250.
- Dicleli, M., & Karalar, M. 2011. Optimum characteristic properties of isolators with bilinear force–displacement hysteresis for seismic protection of bridges built on various site soils. *Soil Dynamics and Earthquake Engineering*, 31(7), 982-995.
- ECS. 2005a. Eurocode 8: Design of structures for earthquake resistance-part 1: general rules, seismic actions and rules for buildings. In: European Committee for Standardization Brussels.
- Elghazouli, A. 2016. *Seismic design of buildings to Eurocode 8*: CRC Press.
- Eröz, M., & DesRoches, R. 2008. Bridge seismic response as a function of the Friction Pendulum System (FPS) modeling assumptions. *Engineering Structures*, 30(11), 3204-3212.
- Fenz, D. M., & Constantinou, M. C. 2006. Behaviour of the double concave friction pendulum bearing. *Earthquake Engineering & Structural Dynamics*, 35(11), 1403-1424.
- Giardini, D. 1999. The global seismic hazard assessment program (GSHAP)-1992/1999. *Annals of Geophysics*, 42(6).
- Giardini, D., Wössner, J., & Danciu, L. 2014. Mapping Europe's seismic hazard. *Eos, Transactions American Geophysical Union*, 95(29), 261-262.
- Guizani, L. 2003. *Sur l'isolation sismique des ponts au Canada*. Paper presented at the 10e Colloque sur la progression de la recherche québécoise sur les ouvrages d'art.
- Guizani, L. 2007. *Isolation sismique et technologies parasismiques pour les ponts au Québec: Mise au point*. Paper presented at the 14e Colloque sur la progression de la recherche québécoise sur les ouvrages d'art.
- Guizani, L., & Chaallal, O. 2011. Mise en conformité sismique des ponts par isolation de la base – Application au pont Madrid au Québec. *Canadian Journal of Civil Engineering*, 38(1), 1-10. Retrieved from <http://www.nrcresearchpress.com/doi/abs/10.1139/L10-104>. doi:10.1139/L10-104
- Huo, Y., & Alemdar, B. N. 2010. Optimal Seismic Isolation Design for A Highway Bridge with Nonlinear Base Isolator Modeling.
- Jangid, R. 2007. Optimum lead–rubber isolation bearings for near-fault motions. *Engineering Structures*, 29(10), 2503-2513.
- Jara, M., Jara, J., Olmos, B., & Casas, J. 2012. Improved procedure for equivalent linearization of bridges supported on hysteretic isolators. *Engineering Structures*, 35, 99-106.
- Koval, V., Christopoulos, C., & Tremblay, R. 2016. Improvements to the simplified analysis method for the design of seismically isolated bridges in CSA-S6-14. *Canadian Journal of Civil Engineering*, 43(10), 897-907.

- Kramer, S. L. 1996. *Geotechnical Earthquake Engineering* Prentice Hall. New York.
- Leroux, M., Tremblay, R., & Léger, P. 2017. A SIMPLIFIED METHOD FOR PRELIMINARY ASSESSMENT OF SEISMIC FORCES IN ISOLATED HIGHWAY BRIDGES WITH MASSIVE PIERS.
- Liu, T., & Zhang, Q. 2016. AP/VP specific equivalent viscous damping model for base-isolated buildings characterized by SDOF systems. *Engineering Structures*, 111, 36-47.
- M. Pagani, J. G.-P., R. Gee, K. Johnson, V. Poggi, R. Styron, G. Weatherill, M. Simionato, D. Viganò, L. Danciu, D. Monelli. 2018. Global Earthquake Model (GEM) Seismic Hazard Map (version 2018.1 - December 2018). doi:10.13117/GEM-GLOBAL-SEISMIC-HAZARD-MAP-2018.1
- Makris, N., & Black, C. J. 2004. Dimensional analysis of rigid-plastic and elastoplastic structures under pulse-type excitations. *Journal of engineering mechanics*, 130(9), 1006-1018.
- Makris, N., & Black, C. J. 2004. Evaluation of Peak Ground Velocity as a "good" intensity measure for near-source Ground Motions. *Journal of Engineering Mechanics*, 130(9), 1032-1044. Retrieved from <https://ascelibrary.org/doi/abs/10.1061/%28ASCE%290733-9399%282004%29130%3A9%281032%29> doi:doi:10.1061/(ASCE)0733-9399(2004)130:9(1032)
- Mavronicola, E., & Komodromos, P. 2011. Assessing the suitability of equivalent linear elastic analysis of seismically isolated multi-storey buildings. *Computers & structures*, 89(21-22), 1920-1931.
- Mavronicola, E., & Komodromos, P. 2014. On the response of base-isolated buildings using bilinear models for LRBs subjected to pulse-like ground motions: sharp vs. smooth behaviour. *Earthq. Struct*, 7(6), 1223-1240.
- MDOC. 2015. Manual de Diseño de Obras Civiles Diseño por Sismo. In: Comisión Federal de Electricidad Mexico.
- Morgan, T. A., & Mahin, S. A. 2011. *The use of base isolation systems to achieve complex seismic performance objectives*: Pacific Earthquake Engineering Research Center.
- Naeim, F., & M. Kelly, J. 1999. *Design of seismic isolated structures : from theory to practice / F. Naeim, J.M. Kelly*.
- Nordenson, G. J., & Bell, G. R. 2000. Seismic design requirements for regions of moderate seismicity. *Earthquake Spectra*, 16(1), 205-225.
- NRC. 10 June 2019. Natural Resources Canada. Retrieved from <http://earthquakescanada.nrcan.gc.ca>
- NRCC. 2015. *National building code of Canada (NBCC)*: National Research Council of Canada, Associate Committee on the National Building Code.
- Ordaz, M., & Meli, R. 2004. Seismic Design Codes in Mexico, on: Proceedings of 13th World Conference on Earthquake Engineering– 13WCEE. *Vancouver, Canada, paper, 4000*.
- Paolucci, R., & Smerzini, C. 2018. Empirical evaluation of peak ground velocity and displacement as a function of elastic spectral ordinates for design. *Earthquake Engineering & Structural Dynamics*, 47(1), 245-255.

- Park, J. G., & Otsuka, H. 1999. Optimal yield level of bilinear seismic isolation devices. *Earthquake Engineering & Structural Dynamics*, 28(9), 941-955.
- Penzien, J., & Watabe, M. 1974. Characteristics of 3-dimensional earthquake ground motions. *Earthquake Engineering & Structural Dynamics*, 3(4), 365-373.
- SeismoSoft. 2016. SeismoMatch 2016. In: Earthquake Engineering Software Solutions Seismosoft Pavia, Italy.
- Solomos, G., Pinto, A., & Dimova, S. 2008. A review of the seismic hazard zonation in national building codes in the context of eurocode 8. *JRC Scientific and Technical Reports*.
- Tarr, A. C., Villaseñor, A., Furlong, K. P., Rhea, S., & Benz, H. M. 2010. *Seismicity of the Earth 1900-2007 (2329-132X)*. Retrieved from
- Tremblay, R., Atkinson, G. M., Bouaanani, N., Daneshvar, P., Léger, P., & Kobojevic, S. 2015. *Selection and scaling of ground motion time histories for seismic analysis using NBCC 2015*. Paper presented at the Proceeding 11th Canadian Conference on Earthquake Engineering, Victoria, BC, Canada, Paper no.
- Trifunac, M., & Todorovska, M. 2012. Earthquake design spectra for performance based design. *Proceedings of the 15WCEE. Paper, 3313*.
- Tubaldi, E., Mitoulis, S., & Ahmadi, H. 2018. Comparison of different models for high damping rubber bearings in seismically isolated bridges. *Soil Dynamics and Earthquake Engineering*, 104, 329-345.
- USGS. 9 June 2019. US Geological Survey, Earthquake Hazards Program. Retrieved from <https://earthquake.usgs.gov/>
- Zhang, J., & Huo, Y. 2009. Evaluating effectiveness and optimum design of isolation devices for highway bridges using the fragility function method. *Engineering Structures*, 31(8), 1648-1660. Retrieved from <http://www.sciencedirect.com/science/article/pii/S0141029609000674>. doi:<http://doi.org/10.1016/j.engstruct.2009.02.017>

Notation

| | |
|----------|--|
| SIS: | seismic isolation system |
| HSA: | high seismicity areas |
| MSA: | moderate seismicity areas |
| LRB: | lead-lug rubber bearing |
| HDRB: | high damping rubber bearing |
| LDRB: | low damping rubber bearing |
| GSHAP: | Global Seismic Hazard Assessment Program |
| GEM: | Global Earthquake Model |
| SIM3064: | Seismicity of the Earth 1900-2007 |
| SHARE: | Seismic Hazard Harmonization in Europe |
| PGA: | peak ground acceleration |
| PGV: | peak ground velocity |
| Sa: | spectral acceleration |
| Sd: | spectral displacement |

Table 1. Amplitude parameters of specific earthquake regions

| | | Location | PGA [g] | PGV [m/s] | PGA/PGV [1/s] |
|-----|-------------------|------------------|---------|-----------|---------------|
| MSA | Northwest EUR | Turin (It) | 0.128 | 0.099 | 12.713 |
| | | La Rochelle (Fr) | 0.085 | 0.064 | 13.093 |
| | | Brussels (Be) | 0.081 | 0.060 | 13.157 |
| | Eastern Canada | Montreal | 0.132 | 0.083 | 15.601 |
| | | Quebec | 0.122 | 0.086 | 13.917 |
| | | Ottawa | 0.102 | 0.068 | 14.715 |
| | Eastern US | Rivière-du-Loup | 0.309 | 0.185 | 16.385 |
| | | Boston | 0.048 | 0.029 | 16.237 |
| | | New York | 0.044 | 0.025 | 17.266 |
| | | Philadelphia | 0.030 | 0.021 | 14.014 |
| HSA | Southeast EUR | Napoli (It) | 0.320 | 0.401 | 7.832 |
| | | Athens (Gr) | 0.391 | 0.500 | 7.677 |
| | | Istanbul (Tr) | 0.535 | 0.706 | 7.440 |
| | Western Canada | Vancouver | 0.189 | 0.263 | 7.050 |
| | | Victoria | 0.306 | 0.393 | 7.638 |
| | Western US | Portland | 0.176 | 0.179 | 9.646 |
| | | Los Angeles | 0.438 | 0.420 | 10.230 |
| | | San Diego | 0.270 | 0.247 | 10.723 |
| | | San Francisco | 0.422 | 0.442 | 9.366 |

Table 2. Spectral accelerations and displacement ratios for different locations in MSAs and HSAs

| | | Location | S _a (0.2) | S _a (2.0) | R _{Sa} | S _d (0.2) | S _d (2.0) | R _{Sd} |
|-----------|------------------------|------------------|----------------------|----------------------|-----------------|----------------------|----------------------|-----------------|
| | | | [g] | [g] | | [mm] | [mm] | |
| MSA | Northwest EU (Type 2) | Turin (It) | 0.317 | 0.024 | 13.33 | 3.15 | 23.7 | 7.50 |
| | | La Rochelle (Fr) | 0.213 | 0.016 | 13.33 | 2.11 | 15.9 | 7.50 |
| | | Brussels (Be) | 0.203 | 0.015 | 13.33 | 2.01 | 15.1 | 7.50 |
| | Eastern Canada | Montreal | 0.206 | 0.024 | 8.58 | 2.06 | 24 | 11.65 |
| | | Quebec | 0.192 | 0.026 | 7.38 | 1.92 | 26 | 13.54 |
| | | Ottawa | 0.161 | 0.020 | 8.05 | 1.61 | 20 | 12.42 |
| | Eastern US | Rivière-du-Loup | 0.483 | 0.043 | 11.23 | 4.83 | 43 | 8.90 |
| | | Boston | 0.129 | 0.021 | 6.13 | 1.28 | 21 | 16.32 |
| | | New York | 0.117 | 0.018 | 6.50 | 1.17 | 18 | 15.38 |
| | Philadelphia | 0.083 | 0.016 | 5.28 | 0.83 | 15.78 | 18.93 | |
| HSA | South East EU (Type 1) | Napoli (It) | 0.801 | 0.200 | 4.00 | 7.96 | 199 | 25.00 |
| | | Athens (Gr) | 0.978 | 0.245 | 4.00 | 9.72 | 243 | 25.00 |
| | | Istanbul (Tr) | 1.338 | 0.335 | 4.00 | 13.30 | 332 | 25.00 |
| | Western Canada | Vancouver | 0.437 | 0.117 | 3.73 | 4.37 | 117 | 26.77 |
| | | Victoria | 0.691 | 0.171 | 4.04 | 6.91 | 171 | 24.75 |
| | Western US | Portland | 0.533 | 0.101 | 4.21 | 5.33 | 158 | 23.78 |
| | | Los Angeles | 1.285 | 0.217 | 4.73 | 12.85 | 339 | 21.13 |
| San Diego | | 0.793 | 0.128 | 4.94 | 7.93 | 201 | 20.24 | |
| | San Francisco | 1.273 | 0.238 | 4.28 | 12.73 | 372 | 23.39 | |

Table 3. Parameters used to represent various SIS characteristics

| SIS parameters | Studied range |
|---|-------------------------------------|
| Elastic stiffness (K_u/W) (m^{-1}) | 25 |
| Characteristic strength ratio (Q_d/W) | 0.02 to 0.1, step increment: 0.001 |
| Post-elastic stiffness (K_d/W) (m^{-1}) | 0.75 to 3.75; step increment: 0.025 |
| Post-elastic ratio ($\mu=K_d/K_u$) | 0.03 to 0.15 |

Table 4. M-R scenarios and the scaling period ranges used for the selected artificial ground motions for Montreal and Vancouver

| Location | Scenario | Magnitude | Distance | Scaling period range |
|-----------|----------|-----------|----------|----------------------|
| Montreal | 1 | M6.0 | R10-R30 | 0.1 – 2.0 [s] |
| | 2 | M7.0 | R20-R70 | 0.5 – 6.0 [s] |
| Vancouver | 1 | M6.5 | R10-R30 | 0.1 – 3.0 [s] |
| | 2 | M7.5 | R25-R100 | 0.5 – 6.0 [s] |

Table 5. Historical ground motions used for Montreal and Vancouver

| Location | Earthquake, station | Mw | R (km) | Component | PGA [g] |
|-----------|---|-----|--------|----------------------|---------|
| Montreal | Nahanni, 23-12- 1985 Bettlement Creek-S3 | 6.5 | 24 | N 270 ⁰ | 0.186 |
| | | | | N 360 ⁰ | 0.194 |
| | Saguenay, 25-11-1988 Chicoutimi-Nord | 5.9 | 43 | N 124 ⁰ | 0.131 |
| | | | | N 214 ⁰ | 0.106 |
| | Van-des-Bois, 23-1-2010 Ottawa | 5.8 | 60 | HHE | 0.028 |
| | | | | HHN | 0.022 |
| Vancouver | Loma Prieta, 17-9-1989 Sans-Francisco-Presidio | 7.0 | 98 | N-S, 0 ⁰ | 0.199 |
| | | | | E-W, 90 ⁰ | 0.100 |
| | Morgan Hill, 24-4-1984 San Ysidro Gilroy #6 | 6.2 | 36 | E-W, 90 | 0.286 |
| | | | | N-S, 360 | 0.219 |
| | Northridge, 17-01-1994 Castaic-Old Ridge Rte | 6.7 | 41 | E-W, 90 | 0.568 |
| | | | | N-S, 360 | 0.514 |

Table 6. Parameters used to optimize SIS characteristics

| Parameter | Value |
|---|-----------------------------------|
| Elastic stiffness (K_e/W) (m^{-1}) | 20, 25, 35, 45, 75, 100 |
| Characteristic strength ratio (Q_d/W) | 0.01 to 0.2, step increment 0.001 |
| Post-elastic stiffness (K_d/W) (m^{-1}) | 0.025 to 5, step increment 0.025 |

Figure captions

Figure 1. Bilinear hysteresis model, typically used for seismic isolators

Figure 2. Design spectra with a probability of exceedance of 10% in 50 years: a) Italy (ECS 2005a); b) Canada (CSA 2014); c) United States (AASHTO 2017); and d) Mexico (MDOC 2015)

Figure 3. Ground motion characteristics in North America and in Europe, background map from GEM (M. Pagni 2018)

Figure 4. Typical seismic-isolated bridge and SDOF model

Figure 5. SMSA scheme for base-isolated bridges with stiff substructures

Figure 6. Mean spectra of scaled historical ground motions and design spectra: a) Vancouver, b) Montreal

Figure 7. Effect of various isolator parameters on F_{\max} and D_{\max} : a) Q_d/W on F_{\max} with $K_d/W=2.5 \text{ m}^{-1}$; b) Q_d/W on D_{\max} with $K_d/W=2.5 \text{ m}^{-1}$; c) K_d/W on F_{\max} with $Q_d/W=0.05$; and d) K_d/W on D_{\max} with $Q_d/W=0.05$

Figure 8. Effect of Q_d/W with different K_d/W on F_{\max} and D_{\max} for isolated bridge: a), c) Vancouver; b), d) Montreal, (K_d/W in m^{-1})

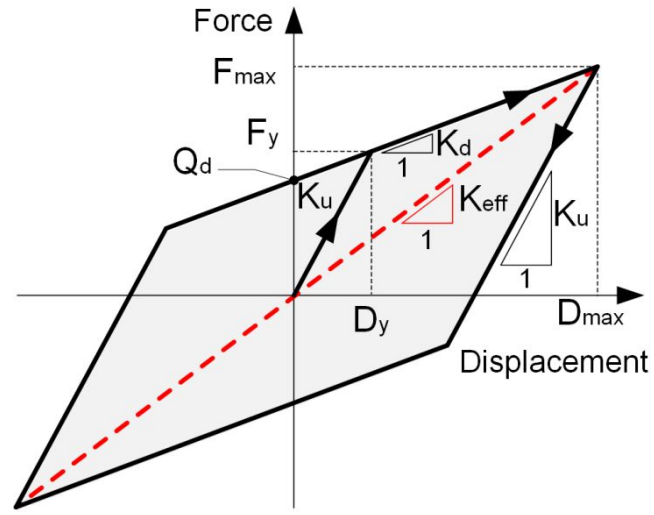
Figure 9. Effect of K_d/W with different Q_d/W on F_{\max} and D_{\max} for isolated bridges: a), c) Vancouver; b), d) Montreal

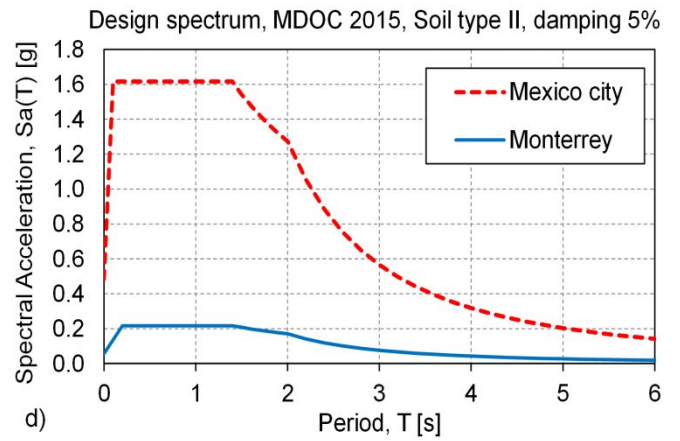
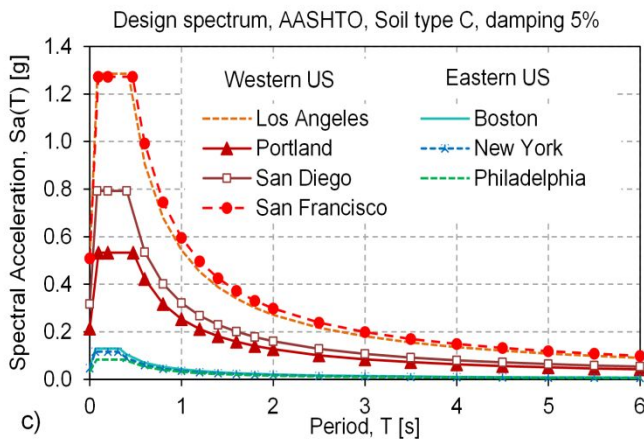
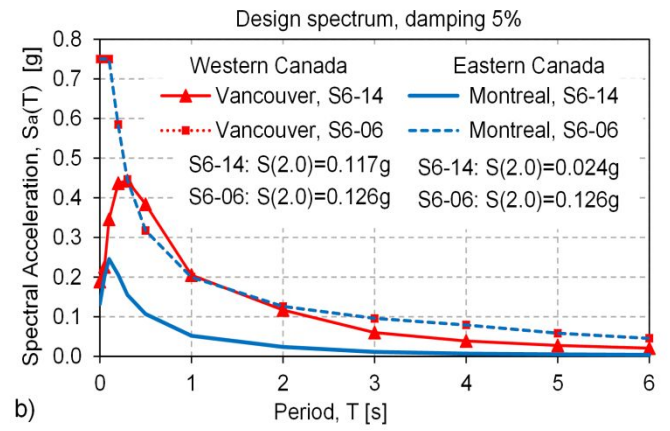
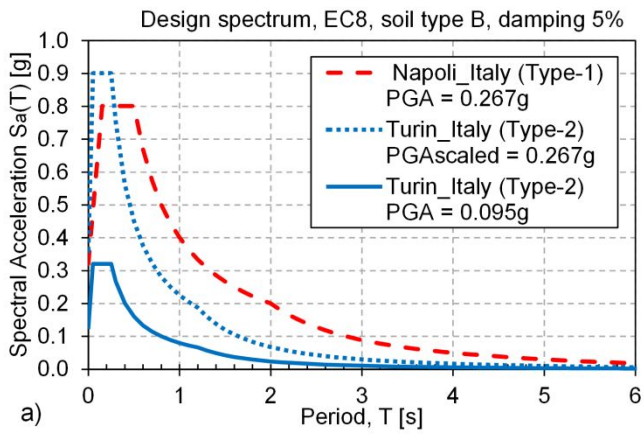
Figure 10. Effect of K_d/W with different Q_d/W on D_r for isolated bridge: a) in Vancouver; b) in Montreal

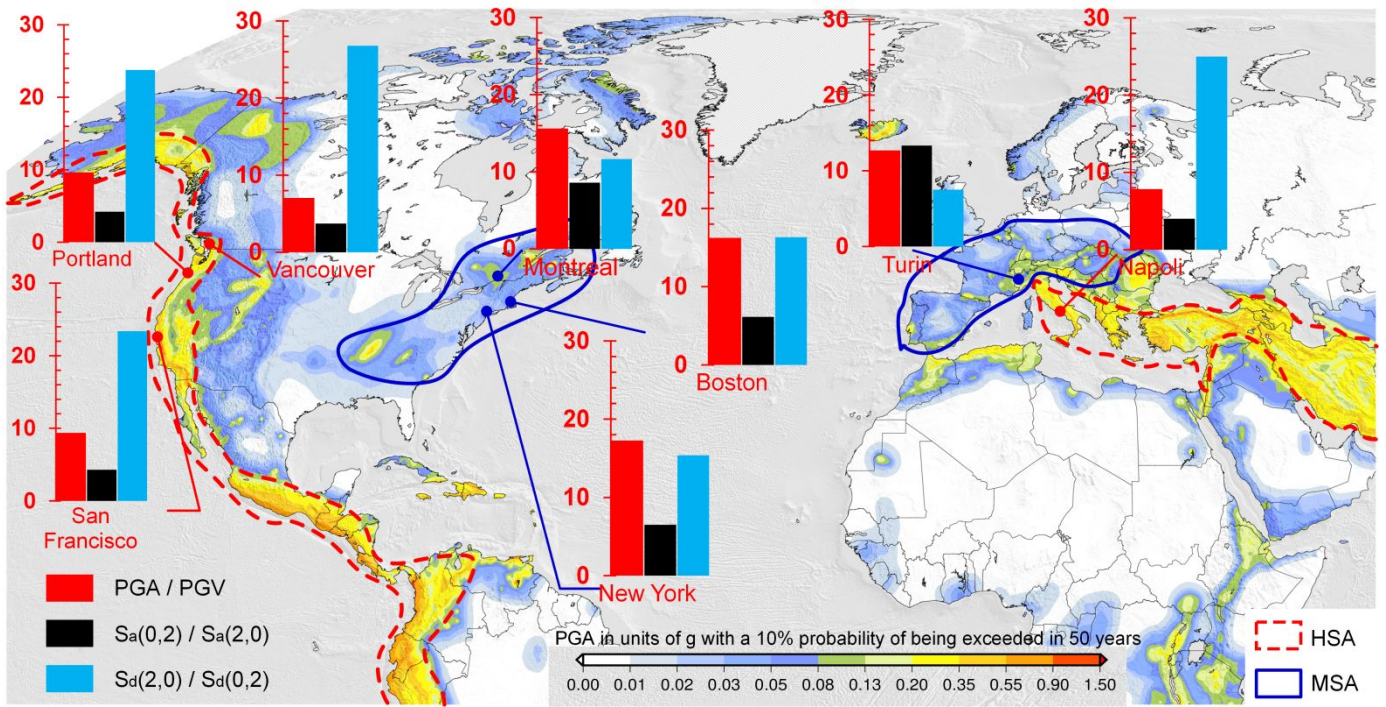
Figure 11. Statistical distribution of Q_d/W minimizing F_{\max} for isolated bridges: a) in Vancouver (HSA), b) in Montreal (MSA)

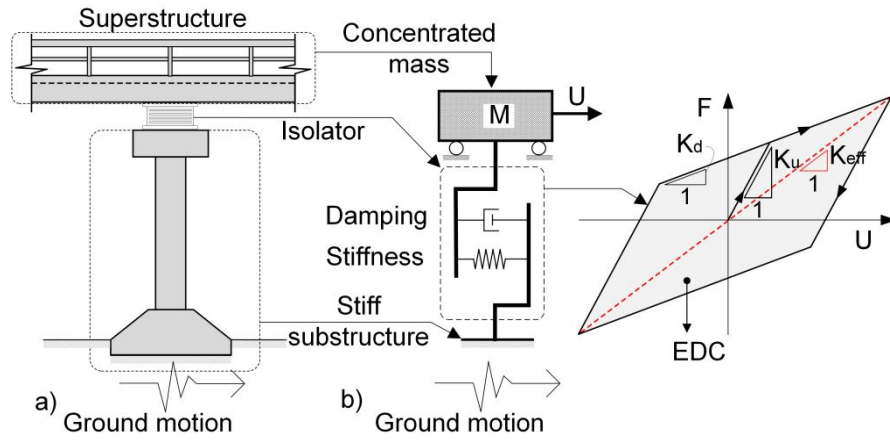
Figure 12. Optimal Q_d/W , minimizing F_{\max} , as a function of K_d/W

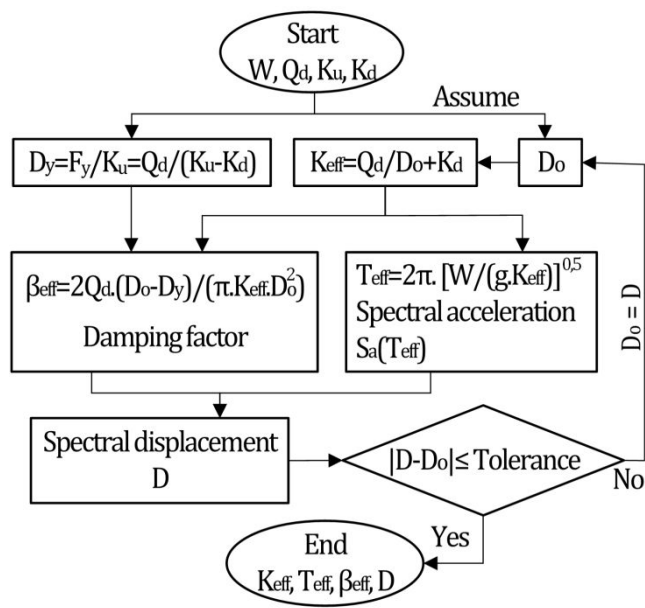
Figure 13. Equivalent viscous damping ratios for Vancouver and Montreal: a) optimal ratios calculated at associated design displacement; b) damping ratios for optimal solutions variation with locality

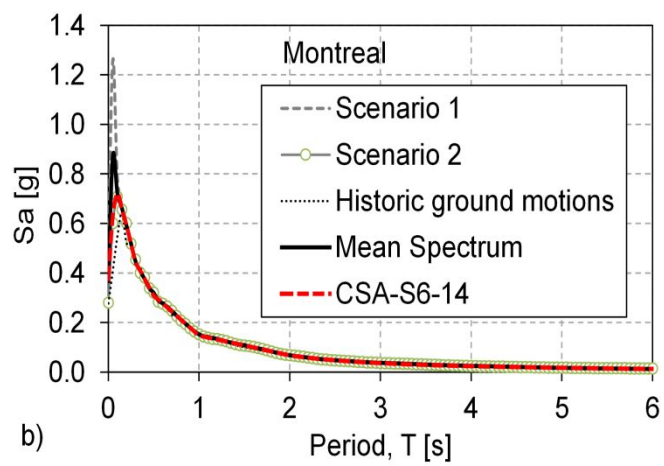
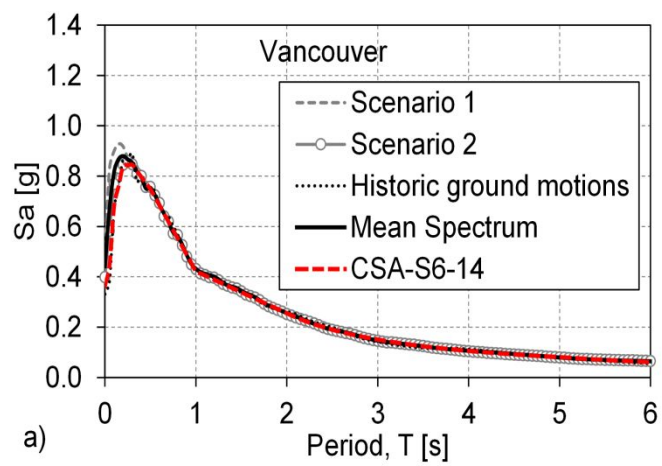


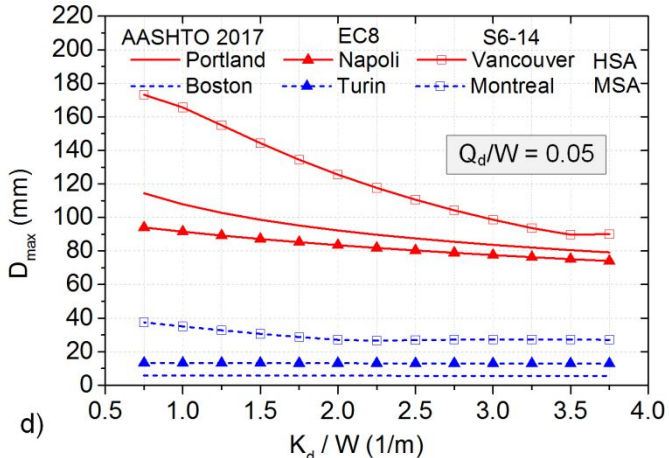
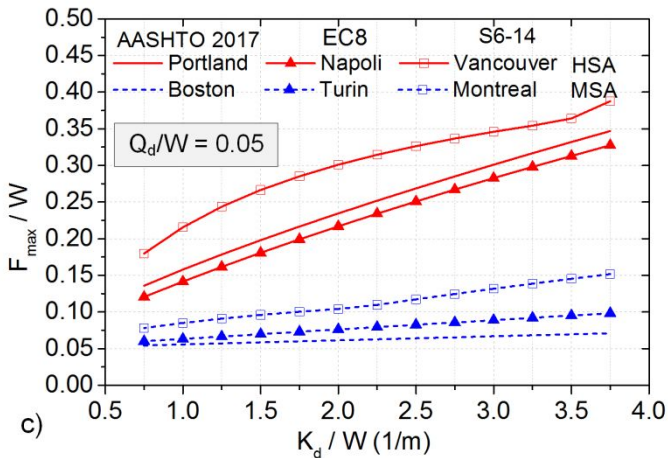
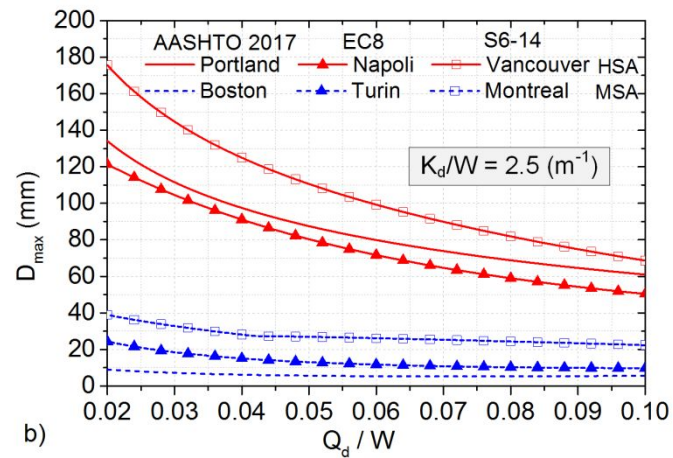
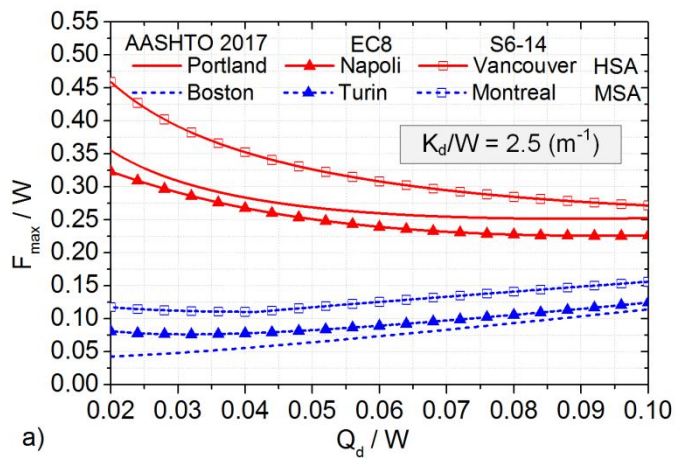


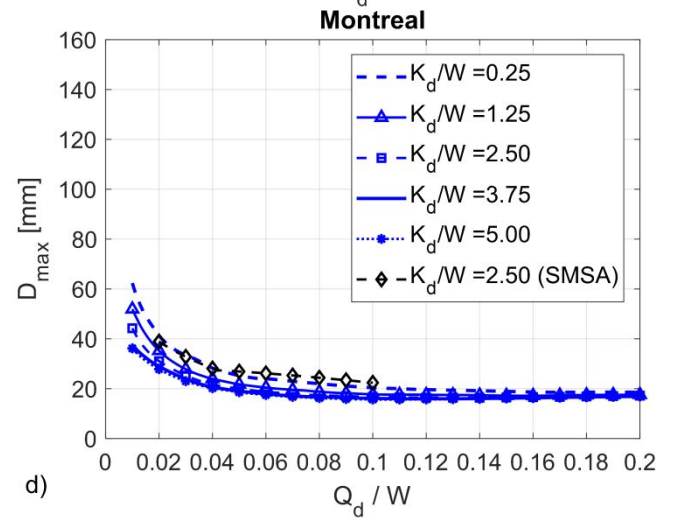
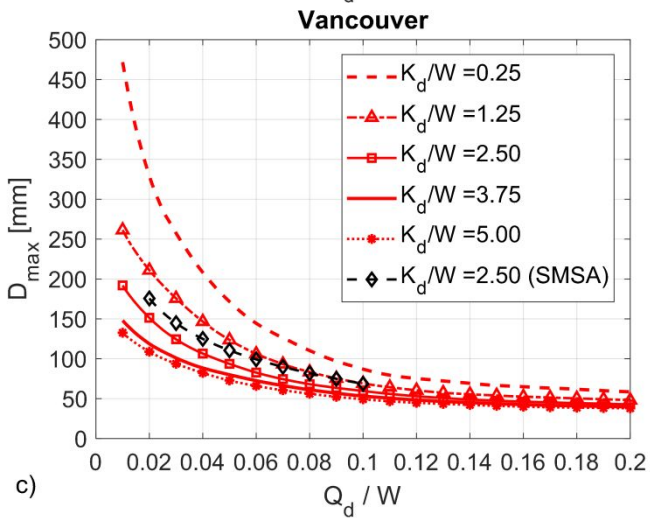
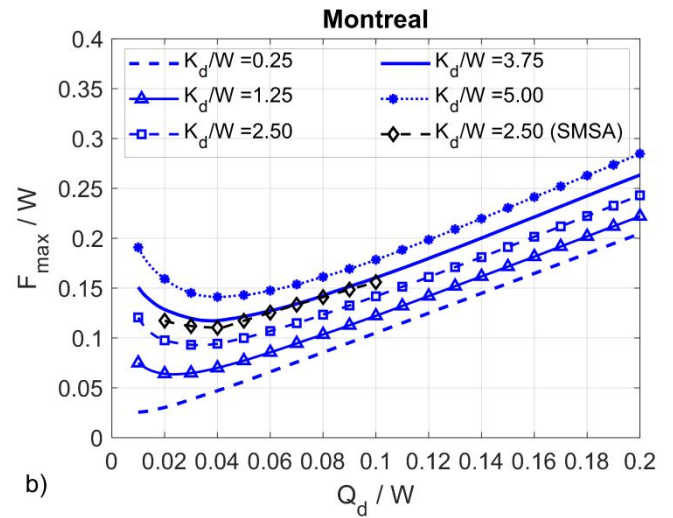
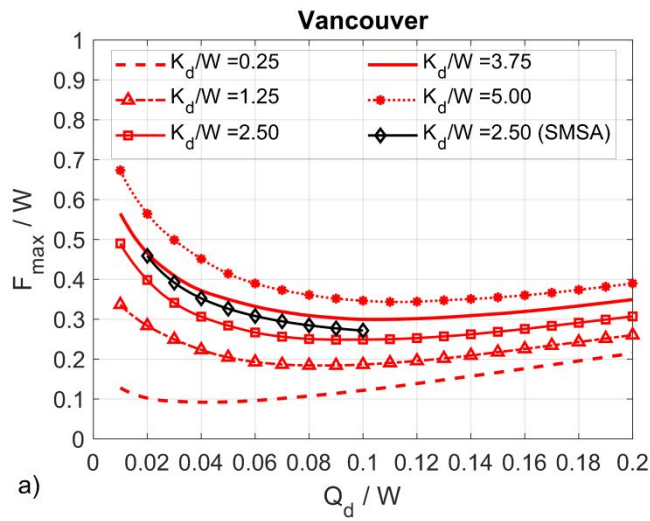












Can. J. Civ. Eng. Downloaded from www.nrcresearchpress.com by National University of Singapore on 05/25/20 For personal use only. This Just-IN manuscript is the accepted manuscript prior to copy editing and page composition. It may differ from the final official version of record.

